https://doi.org/10.5194/egusphere-2026-462
Preprint. Discussion started: 19 February 2026

Impact of climate forcing time step on the modelled ice-sheet firn layer

Tesse E. A. van den Aker[1], Peter Kuipers Munneke[1], Willem Jan van de Berg[1], Walter W. Immerzeel[2], and Michiel R. van den Broeke[1]

[1]Institute for Marine and Atmospheric Research, Utrecht University, Utrecht, the Netherlands
[2]Department of Physical Geography, Utrecht University, Utrecht, The Netherlands

Correspondence: Tesse E. A. van den Aker (t.e.a.vandenaker@uu.nl)

Abstract. The firn layer regulates how an ice-sheet responds to climate change by modifying how changes in surface temperature, snow accumulation and ablation affect the ice-sheet mass balance. Firn properties are often simulated with a firn densification model. Firn models are forced with surface mass balance components, surface energy balance components and/or meteorological variables. In literature, a variety of time steps in those climate forcings have been used to force such firn models, ranging from 3-hours to 1-day, 1-month, or even annual. To investigate the impact of these different time steps, we force the firn densification model IMAU-FDM with different climate forcing time steps at the surface for the Antarctic Peninsula and southern Greenland Ice Sheet. We show that the modelled firn layer contains more pore space for larger forcing time steps, and that locations with limited firn pore space due to seasonal melt are most sensitive. The climate forcing time step impacts the creation of pore space by snowfall and the depletion of pore space by snowmelt and firn densification. The key in causing the differences in firn pore space is the presence or absence of a diurnal cycle in the input data. A climate forcing time step greater than a day allows for a non-physical coexistence of snowmelt and sub-zero surface temperatures, leading to immediate shallow refreezing of meltwater. Subsequent melting removes refrozen ice rather than porous firn, reducing the amount of firn air that is lost through melting. Therefore, the decoupled temperature and snowmelt in the upper layers give more firn air with a climate forcing time step larger than a day. We also found that firn density parameterizations can become unsuitable when applied outside the physical conditions or climate forcing time step on which they are based. These parameterizations lead to unrealistic firn densification and accumulation behavior in the model. We argue that (1) firn models require a timestep small enough to capture at least the diurnal cycle, (2) use of parameterizations should be critically assessed and used consistently with the way they were originally developed, and (3) the forcing time step should be considered when interpreting firn model output.

1 Introduction

Firn, the transitional state between snow and glacial ice, covers $\sim 90\%$ of the Greenland Ice Sheet (GrIS) (Noël et al., 2022) and $\sim 99\%$ of the Antarctic Ice Sheet (AIS) (Winther et al., 2001). Firn contains air that prevents a fraction of the meltwater to run off into the ocean, either by refreezing or retention. Approximately $\sim 39\%$ of surface meltwater on the GrIS and $\sim 94\%$

https://doi.org/10.5194/egusphere-2026-462
Preprint. Discussion started: 19 February 2026

Table 1. Overview of the variety in climate forcing time steps used in different firn models.

Climate forcing time step	Literature
1-hour	Community Firn Model (CFM) (Medley et al., 2022; Thompson-Munson et al., 2023), SNOWPACK (Thompson-Munson et al., 2023; Wever et al., 2023)
3-hours	CFM (Verjans et al., 2019; Vandecrux et al., 2020), DTU model, HIRHAM, MeyerHewitt, UppsalaUniBucket, GEUS model (Vandecrux et al., 2020), IMAU-FDM (Vandecrux et al., 2020; Brils et al., 2021; Veldhuijsen et al., 2023)
6-hours	HIRHAM (Langen et al., 2017; Hansen et al., 2024)
1-day	Firn densification model based on CFM (Zhang et al., 2024)
1-month	DTU model (Sørensen et al., 2011; Simonsen et al., 2013), CFM (Stevens et al., 2020; Gkinis et al., 2021)
1-season	MeyerHewitt (Meyer and Hewitt, 2017)
Annual	CFM (Gkinis et al., 2021)

on the AIS is retained in the firn (Medley et al., 2022). Consequently, the firn layer keeps meltwater away from crevasses on Antarctic ice shelves, where it could otherwise engage in hydrofracturing. Also, outside the percolation zone the firn layer evolution is of relevance, as variations in firn mass and thickness complicate the interpretation of altimetry observations for ice-sheet mass balance.

Firn models are used to improve our understanding of physical processes, to interpret observations, to interpret remote sensing data, and to assess ice-sheet surface mass balance (SMB) in the future (The Firn Symposium team, 2024). Firn models differ in their parameterizations and formulations for densification, thermodynamics, and water percolation processes (Vandecrux et al., 2020). Although a variety of firn models exist, all models have in common that they use numerical methods to integrate a set of coupled differential equations in time. In this paper, we focus on the fact that the upper boundary conditions for solving the equations are provided at a discrete time step. Those boundary conditions can be components of the SMB and/or surface energy balance (SEB), or meteorological variables, which varies depending on the firn model (The Firn Symposium team, 2024). The climate forcing time step differs greatly across studies (Table 1), varying from 1 hour, to days, months, and even years.

Reasons for choosing a certain climate forcing time step are most often practical: the data are not available at smaller time steps, the amount of forcing data becomes too large, or the computational resources are insufficient. Evaluation of the forcing time step is often absent or based on differing lines of reasoning. For example, Medley et al. (2022) argue that the absence of a diurnal cycle in the forcing time step is a limitation of their model, whereas Meyer and Hewitt (2017) expect that the daily cycle influences only the uppermost meter of the firn column, and therefore, ignore it. We want to emphasize the difference between the time step used to solve the differential equations in a model, and the time step at which the forcing data is provided. The

https://doi.org/10.5194/egusphere-2026-462
Preprint. Discussion started: 19 February 2026

focus of this paper is on the latter. Most often, the model time step is smaller than the forcing data time step. To clarify with an example, Veldhuijsen et al. (2023) uses a 3-hourly climate forcing linearly interpolated to a 15 minute model time step.

In this paper, we aim demonstrate that the output of a firn model is sensitive to the forcing time step when forced with SMB and meteorological variables at the surface, while focusing on the Antarctic Peninsula Ice Sheet (APIS) and the southern GrIS.

2 Methods: Firn modelling setup

We use the IMAU Firn Densification Model (IMAU-FDM) (Brils et al., 2021; Veldhuijsen et al., 2023). This section describes IMAU-FDM and specifies similarities and differences in the model for the two domains. We also describe the forcing dataset, model initialization, the setup for testing different forcing time steps, and the study areas.

2.1 IMAU-FDM

IMAU-FDM is a 1D semi-empirical model that simulates densification rate, refreezing, temperature evolution, and meltwater transport in the firn layer. The model is developed by Helsen et al. (2008) and has undergone multiple updates (Ligtenberg et al., 2014; Brils et al., 2021; Veldhuijsen et al., 2023). We use IMAU-FDM v1.2A (Veldhuijsen et al., 2023) for the Antarctic domain and IMAU-FDM v1.2G (Brils et al., 2021) for the Greenland domain, which only differ from each other in their ice-sheet dependent calibration. Both versions have been evaluated extensively against firn density and temperature observations (Ligtenberg et al., 2014; Kuipers Munneke et al., 2015; Brils et al., 2021; Veldhuijsen et al., 2023).

The firn and ice column are divided into 200 to 3,000 layers, traced in a Lagrangian framework. Snowfall is added to the topmost layer of the column, burying other layers and thereby representing downward advection. No layers are removed during a simulation. The layers have a maximum vertical resolution of 0.15 m. Layer routines are build in that split the uppermost layer if it exceeds the 0.15 m threshold and merges the two uppermost layers if the thickness of the uppermost layer is smaller than 0.05 m. When the firn column has less than 200 layers, 100 very thin layers of pure ice are added to the bottom of the column.

The fresh snow density is an upper boundary condition with differing parameterizations for the AIS and GrIS domain. In IMAU-FDM v1.2A (AIS), the fresh snow density ρ_0 (kg m^{-3}) depends on instantaneous surface temperature T_s (K) and 10 m wind speed ff_{10m} (m/s) (Eq. 1) (Lenaerts et al., 2012; Veldhuijsen et al., 2023):

$$\rho_0 = 82.97 + 0.769 T_s + 11.67 ff_{10m} \tag{1}$$

In IMAU-FDM v1.2G (GrIS), ρ_0 is based on the surface temperature averaged over the year prior to the snowfall $\overline{T_s}$ (K) (Eq. 2) (Fausto et al., 2018; Brils et al., 2021):

$$\rho_0 = 362.1 + 2.78(\overline{T_s} - 273.15) \tag{2}$$

https://doi.org/10.5194/egusphere-2026-462
Preprint. Discussion started: 19 February 2026

The snow and underlying firn densification in each layer is parameterized by a semi-empirical equation (Eq. 3) based on Arthern et al. (2010):

$$\frac{d\rho}{dt} = D\dot{b}gMO(\rho_i - \rho)e^{-\frac{E_c}{RT}+\frac{E_g}{RT_b}} \tag{3}$$

with $\dot{b}$ the average accumulation rate (kg m^{-2} yr^{-1}) over the spin-up period, g the gravitational acceleration (9.81 m s^{-2}), ρ_i the density of bubble-free ice (917 kg m^{-3}), ρ the instantaneous layer density (kg m^{-3}), E_c the activation energy for creep (60,000 J mol^{-1}), E_g the activation energy for grain growth (42,400 J mol^{-1}), R the universal gas constant (8.3145 J mol^{-1}K^{-1}), T the instantaneous layer temperature (K), and T_b the instantaneous temperature of the bottom firn layer. D is a constant and MO is a correction term that improves model alignment with observations at depths of the 550 and 830 kg m^{-3} density levels (Ligtenberg et al., 2011). The correction term differs for both domains (Brils et al., 2021; Veldhuijsen et al., 2023). In this equation, $e^{-E_c/(RT)}$ represents the temperature-dependency of ice deformation; $e^{E_g/(RT_b)}$ is a correction term arising from the estimated grain size ($E_c > E_g$). Ice grains grow faster in warmer conditions, while large grains deform slower than smaller grains, hence reducing the densification. As the current grain size is the result of the grain growth since deposition, its impact on densification must be approximated by the typical temperature conditions. Therefore, the mean firn temperature, estimated by the temperature of the lowermost layer (T_b) is used in Eq. (3).

The physical description for water percolation and thermodynamics is identical in both model versions. Liquid water is added to the top of the column. Its transport through the layers is calculated using the 'bucket scheme'. In this scheme, each layer has an irreducible water content which is the maximum amount of water that can be retained in the layer by capillary forces. The irreducible water content decreases with increasing density (Coléou and Lesaffre, 1998). Water refreezes when enough cold content is available. This formulation implies that, in one model time step, water can percolate through the whole firn layer until it reaches the firn-ice interface. Any leftover water is assumed to run off.

Heat conduction through the firn layer is described by the 1D heat transfer equation, with conductivity being a function of density (Calonne et al., 2019; Brils et al., 2021). Refreezing acts as a heat source within the firn. Heat transfer at the upper boundary is governed by the prescribed surface temperature. A constant heat flux through the bottom layer is applied as the lower boundary condition.

2.2 Forcing dataset

IMAU-FDM is forced at the surface with surface temperature, 10 m windspeed, snowmelt, snowfall, sublimation, snowdrift erosion, and rainfall. These climate forcings originate from the regional atmospheric climate model RACMO2.3p2 (Noël et al., 2018; Van Wessem et al., 2018), dynamically downscaling ERA5 reanalysis data (Hersbach et al., 2020). The AIS/APIS data covers the period 1979 - 2023 with a horizontal resolution of 27 × 27 km^2 (Van Wessem et al., 2018). The GrIS data spans 1 September 1939 - 1 December 2023 with a horizontal resolution of 5.5 × 5.5 km^2 and is a renewed and extended version of the simulation presented by Noël et al. (2018).

https://doi.org/10.5194/egusphere-2026-462
Preprint. Discussion started: 19 February 2026

2.3 Initialization

The firn layer is initialized by spinning up the model over a repeated reference period until it reaches a steady state where the firn air content (FAC) and elevation no longer change. The full firn layer, up to the pore close-off density of 830 kg m^{-3}, is refreshed during the initialization. As a prerequisite, this reference period should not exhibit large climate trends. The AIS/APIS simulation spin-up period covers 1979 - 2020 (Veldhuijsen et al., 2023). After 2020, Antarctica has gained mass due to unprecedented precipitation (Wang et al., 2023), and therefore 2020 - 2023 is excluded from the spin-up period. The GrIS SMB has been decreasing since 1990 (Shepherd et al., 2012). Therefore, we chose the first 30 years of the run (1 September 1939 - 31 December 1970) as the reference period.

2.4 Climate forcing time step

We force the model with four climate forcing time steps (i.e. dt^{force}) at the surface: 3-hours, 6-hours, 1-day and 1-month, referred to as dt_{3h}^{force}, dt_{6h}^{force}, dt_{1d}^{force}, and dt_{1m}^{force} respectively. We chose these values because (1) they are typically used to force firn models (Table 1), and (2) they provide examples with and without a diurnal cycle in the input data (Fig. 1). In addition, dt_{3h}^{force} is the smallest available climate forcing time step from RACMO2.3p2 and is commonly used to force IMAU-FDM. We averaged the 3-hourly surface mass fluxes, surface temperature, and 10 m wind speed data to get the input data for dt_{6h}^{force}, dt_{1d}^{force}, and dt_{1m}^{force}. IMAU-FDM interpolates the forcing data onto a 15-minute model time step in which we assume a constant value for the whole forcing period for the surface mass fluxes, surface temperature and 10 m wind speed (Fig. 1).

2.5 Study areas: APIS and southern GrIS

We select the APIS and the southern GrIS, two areas with a broad range of surface climate conditions, from low to high snowfall and with and without melt (Fig. 2).

In the APIS, the main climate gradient is from the wet and warm west to the dry and cold east. The ice shelves are the lowest-lying areas (Fig. 2a) and experience most snowmelt (up to 500 kg m^{-2} yr^{-1}) (Fig. 2b), whereas the snowmelt is limited on the higher-elevated grounded ice. In contrast, the grounded ice has more accumulation, peaking in the north-west of the APIS. Accumulation is less on the ice shelves (Fig. 2c).

In the southerns GrIS, the lowest-lying marginal areas (Fig. 2d) experience most snowmelt (>750 kg m^{-2} yr^{-1}) (Fig. 2e). Accumulation is highest in the east (> 2000 kg m^{-2} yr^{-1}) (Fig. 2f). The combination of exceeding 500 kg m^{-2} yr^{-1} snowmelt and high accumulation, like in the southeastern GrIS, can result in the presence of firn aquifers, or, in drier climate zones like the southwest, in ice slab formation (Brils et al., 2024).

https://doi.org/10.5194/egusphere-2026-462
Preprint. Discussion started: 19 February 2026

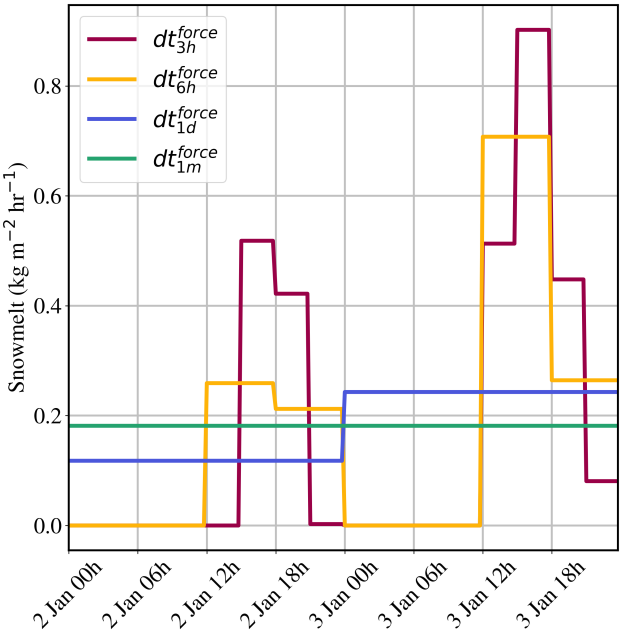

Figure 1. Example of 48 hours of snowmelt forcing at dt_{3h}^{force}, dt_{6h}^{force}, dt_{1d}^{force}, and dt_{1m}^{force}. The graph also visualizes the model's interpolation of the forcing onto a 15-minute timestep. Note the presence of a diurnal cycle in the snowmelt input for dt_{3h}^{force} and dt_{6h}^{force} and its absence for dt_{1d}^{force} and dt_{1m}^{force}.

3 Effect of climate forcing timestep on firn

We look into the FAC patterns for dt_{3h}^{force} and compare this to FAC with larger dt^{force}. We show that increasing dt^{force} leads to more firn pore space. We then identify the processes responsible for these differences. We discuss how these processes depend on the dt^{force} and how this affects the depletion or creation of pore space.

In the discussion of these results, we use the following abbreviations: FAC_{3h}, FAC_{6h}, FAC_{1d}, and FAC_{1m} correspond to the FAC at dt_{3h}^{force}, dt_{6h}^{force}, dt_{1d}^{force}, and dt_{1m}^{force} respectively. The FAC_{3h} compared to FAC simulated at a larger dt^{force}, is defined as $\Delta FAC_{6h} = FAC_{6h} - FAC_{3h}$, $\Delta FAC_{1d} = FAC_{1d} - FAC_{3h}$, and $\Delta FAC_{1m} = FAC_{1m} - FAC_{3h}$. ΔFAC (without subscript) denotes the difference between FAC_{3h} and FAC modelled with larger dt^{force}. A positive ΔFAC indicates more pore space for the climate forcing time step larger than 3-hours.

3.1 FAC_{3h} and ΔFAC

Figure 3 shows the FAC_{3h} (Figs. 3a and e), ΔFAC_{6h} (Figs. 3b and f), ΔFAC_{1d} (Figs. 3c and g), and ΔFAC_{1m} (Figs. 3d and h) for the APIS and southern GrIS. Panels 3b, c, d, f, g, and h show that FAC_{3h} is lower than FAC with larger dt^{force} in both the APIS and southern GrIS. The larger the dt^{force} becomes, the higher the ΔFAC.

https://doi.org/10.5194/egusphere-2026-462
Preprint. Discussion started: 19 February 2026

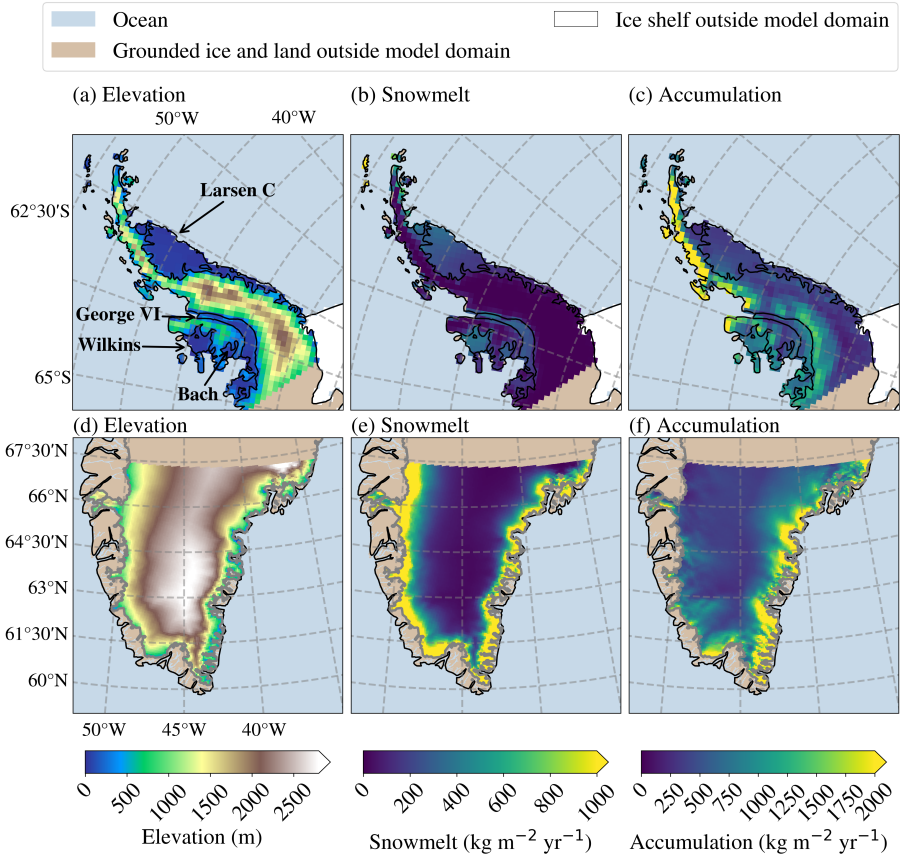

Figure 2. Maps showing elevation (a, d), snowmelt averages (b, e), and accumulation averages (c, f) for the modelled domain in the APIS (a–c) and southern GrIS (d–f) during the spin-up period, i.e. 1979 - 2020 for the APIS and 1 September 1939 – 31 December 1970 for the southern GrIS. The black contours show the coastal and ice shelf boundaries in the APIS (a-c) and the coastal boundaries in the southern GrIS (d-f). Ice shelf names within the model domain are indicated for the APIS (a). Gray contours show the ice mask boundaries in southern GrIS (d-f).

On the APIS, FAC is smallest (0-5 m for FAC_{3h}) in the lower-lying areas, corresponding to the ice shelves (Fig. 3a). ΔFAC is largest on the ice shelves (15 % for ΔFAC_{1d}, increasing up to 44% for ΔFAC_{1m}). ΔFAC_{6h} is relatively small (3%). Interestingly, an area with a negative ΔFAC is situated along the high-elevation southern spine of the APIS (red hues in Figs. 3b, c, and d). In a relative sense, these differences are small, of the order of ~ 0.5 m on typical FAC_{3h} values of 15-20 m. In both an absolute and a relative sense, ΔFAC is largest for the locations with low FAC_{3h}.

In the southern GrIS, FAC increases from the ice margin where it equals zero in the ablation zone, to higher elevations, with the steepest spatial gradients on the east coast (Fig. 3e). In the southern GrIS, in the ablation zone, most clearly visible on the western margin, ΔFAC is small (Figs. 3f, g, and h). Here, firn pore space is depleted across all simulations, regardless of dt^{force}. At high elevations (>2000 m), ΔFAC is also relatively small, with average differences $< 1\%$ in ΔFAC_{6h} up to 3%

https://doi.org/10.5194/egusphere-2026-462
Preprint. Discussion started: 19 February 2026

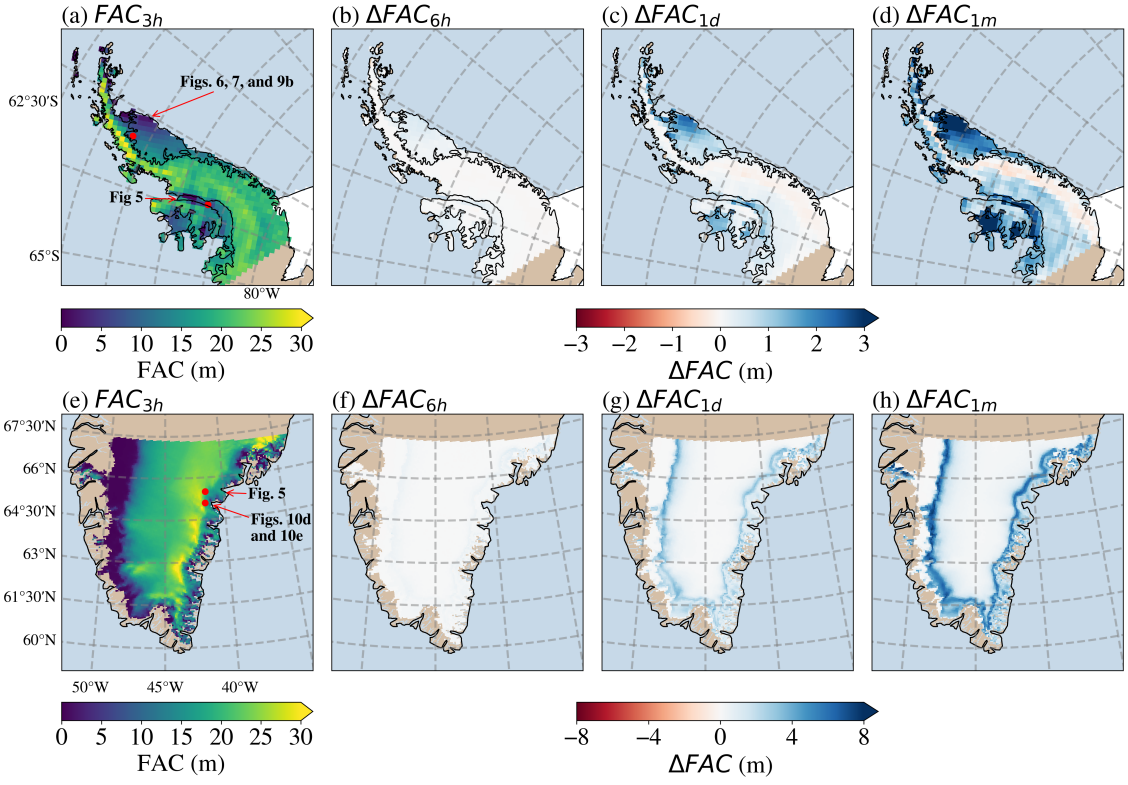

Figure 3. Maps showing average FAC_{3h} (a, e), along with average ΔFAC_{6h} (b, f), ΔFAC_{1d} (c, g), and ΔFAC_{1m} (d, h) in the APIS (a-d) and southern GrIS (e-h). The averages are over the whole simulation period, i.e. 1979 - 2023 for the APIS and 1 September 1939 – 31 December 2023 for the southern GrIS. The points highlighted in panel (a) and (e) are used as an example later in this paper.

in ΔFAC_{1m}. At intermediate elevations, a band with larger ΔFAC is apparent, increasing with greater dt^{force} (Fig. 3f, g, and h). In the east and west, ΔFAC in this band is quite similar in an absolute sense: on average, ΔFAC_{6h} = 0.3 m, ΔFAC_{1d} = 2.1 m, and ΔFAC_{1m} = 4.0 m. However, relative differences are larger in the west, where absolute FAC_{3h} values are much smaller (typically $<$ 20 m) than in the east (typically $>$ 20 m).

3.2 Dominant processes

We discuss the processes that contribute to ΔFAC. Figure 4 gives an overview of the dominant processes in a firn layer that introduce the forcing time step dependency of the FAC and that are described in depth later in this section.

FAC is governed by a balance between the process that create pore space (snowfall) and the processes that deplete it (densification, snowmelt, snowdrift erosion, and sublimation). Figure 5 shows the relative importance of several processes determining FAC_{3h} and FAC_{1d} for two example locations depicted in Fig. 3. Figure 5a represents a location in the APIS and Fig. 5b a location in the southern GrIS. Both locations experience similar melt and ΔFAC_{1d}, but the location in the GrIS has more snow-

https://doi.org/10.5194/egusphere-2026-462
Preprint. Discussion started: 19 February 2026

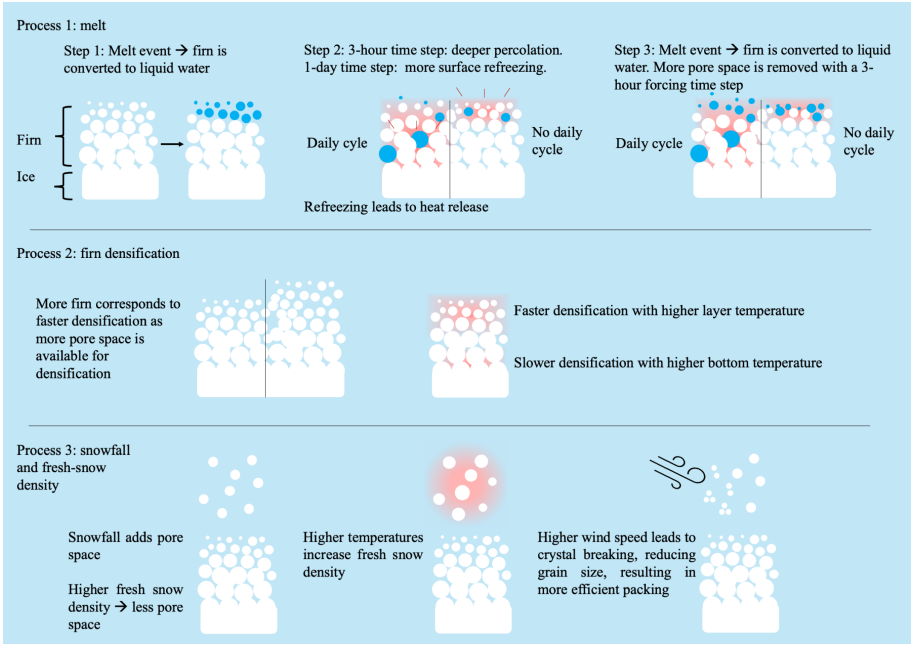

Figure 4. Processes that control the (Δ)FAC.

fall. For clarity, a positive excursion of the elevation change difference in panels 5c and d means that the elevation increases more for dt_{1d}^{force}.

Snowfall is the major source of firn air in both locations (Figs. 5a and b). The contribution of snowfall to FAC for the APIS is slightly higher for dt_{3h}^{force} than dt_{1d}^{force} (Fig. 5c), whereas it is almost the same for the GrIS (Fig. 5d). Larger differences arise for processes that reduce FAC. In both locations, more FAC_{3h} is removed by snowmelt than FAC_{1d} (Figs. 5c and d). For the dry location (Fig. 5a), densification is relatively slow, and FAC depletion due to melt is largest. For the wet location (Fig. 5b), the densification dominates reduction of the FAC. At both locations, melt removes more FAC_{3h} and has slower firn densification at dt_{3h}^{force} (Figs. 5c and d).

Summarizing, ΔFAC is mainly controlled by melt and densification rate, with a minor contribution from snowfall. Now, we further zoom in on those processes to understand the ΔFAC they cause.

3.2.1 Process 1: melt

Melt provides the largest contribution to ΔFAC, simulations with dt_{3h}^{force} have more FAC reduction than for larger dt^{force} (Figs. 5c and d). Climate zones with more melt, have a higher ΔFAC. We identify two types of melt-related mechanisms responsible for ΔFAC, namely a surface-based process and a process occurring at depth.

At the surface, the model is forced with a melt flux. As melt is not generated within the model, firn in the top layer is converted to liquid water (Fig. 4, process 1, step 1). The subsequent fate of the meltwater depends on dt^{force}. With a diurnal cycle in

https://doi.org/10.5194/egusphere-2026-462
Preprint. Discussion started: 19 February 2026

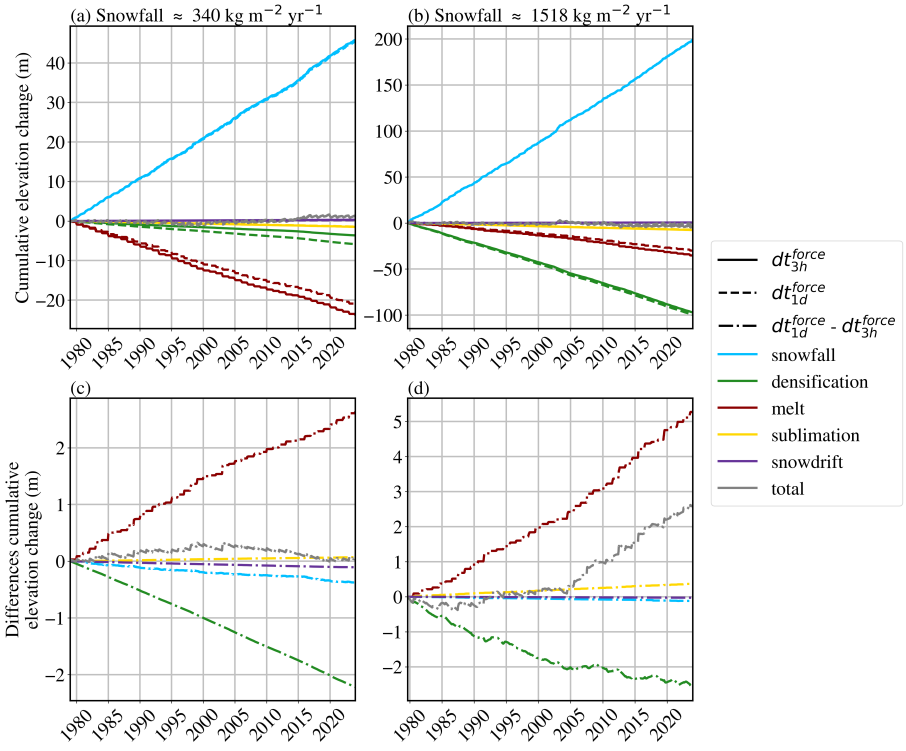

Figure 5. (a) and (b) Cumulative elevation change (m) due to the processes that influence the firn layer. (c) and (d) differences in cumulative elevation change between dt_{1d}^{force} and dt_{3h}^{force}. Firn densification is integrated over the whole firn column. All other variables represent surface processes. Results for dt_{3h}^{force} are in solid lines, for dt_{1d}^{force} are in dashed lines, and the difference between the two is in dash dot lines. Panel (a) and (c) are a location in the APIS and panel (b) and (d) are a location in southern GrIS. Both locations experience similar melt ($\sim$ 340 kg m^{-2} yr^{-1}) and ΔFAC_{1d} (2.1 m), but different snowfall. See Fig. 3a and e for a map with the grid cell locations.

dt^{force}, i.e. 3- and 6-hours, surface temperatures reach 0°C during melt events. Therefore, the water cannot immediately refreeze and the timing of refreezing and snowmelt in the top layer alternate between day and night (Fig. 6a). In contrast, without a diurnal cycle in dt^{force}, i.e. 1-day and 1-month, surface melt and temperature become decoupled. As a result, melt can occur at subfreezing surface temperatures and meltwater refreezes immediately near the surface (Fig. 6b and Fig. 4, process 1, step 2). This leads to a higher near-surface density (more ice) under larger dt^{force} (Fig. 6c). Subsequent melt events convert firn to liquid water again and remove less pore space when a high-density surface layer is present, as in dt_{1d}^{force} and dt_{1m}^{force} (Fig. 4, process 1, step 3). This melt and surface temperature interaction in absence of a daily cycle is the main mechanism that leads to higher ΔFAC with increasing dt^{force}.

The second process is that meltwater percolates deeper at dt_{3h}^{force} (Figs. 7a and b and Fig. 4, process 1, step 2); less water is immediately refrozen near the surface. Consequently, refreezing occurs deeper if there is enough cold content. The latent heat released by refreezing at depth is largely retained due to the low thermal conductivity of firn. Thus, the deeper firn for dt_{3h}^{force}

https://doi.org/10.5194/egusphere-2026-462
Preprint. Discussion started: 19 February 2026

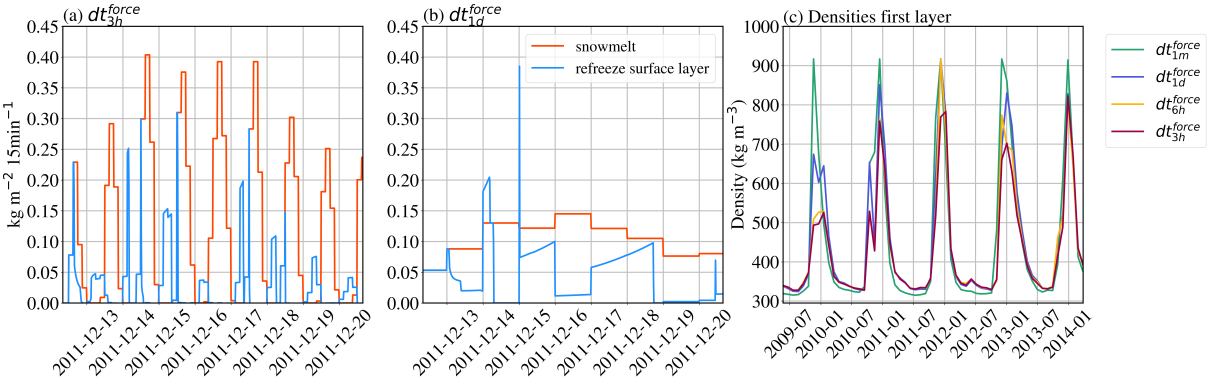

Figure 6. Modelled snowmelt and refreezing in the surface layer for dt_{3h}^{force} (a) and for dt_{1d}^{force} (b). Panel (c) shows the densities in the surface layer. See Fig. 3a for a map with the grid cell location.

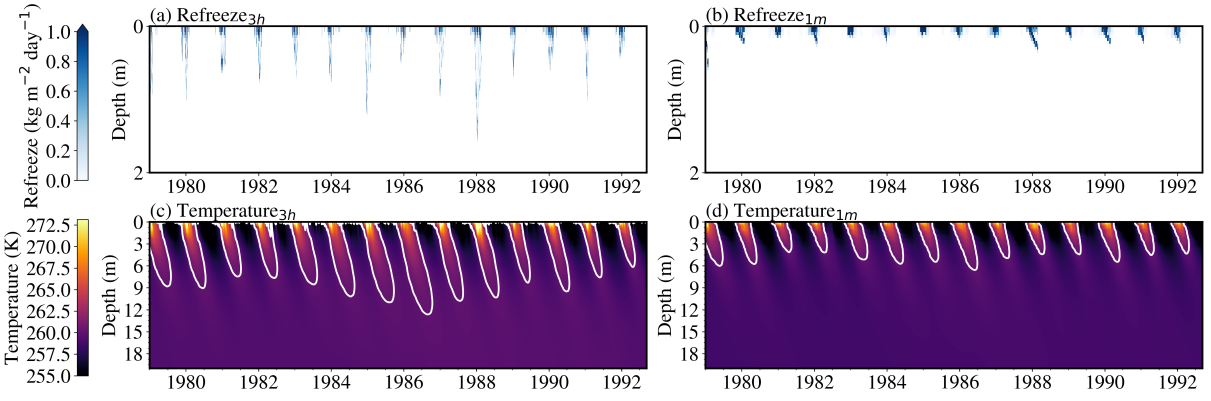

Figure 7. Refreezing amount and depth (a, b) and temperature profiles (c, d) for an example point on the APIS for dt_{3h}^{force} (a, c) and for dt_{1m}^{force} (b, d). The white contours in panels c and d represent a temperature of 260 K. See Fig. 3a for a map with the grid cell location.

is warmer (Figs. 7c and d and Fig. 4, process 1, step 2). Warmer firn enhances firn densification, as discussed in the following subsection.

3.2.2 Process 2: firn densification

Several processes contribute to the firn densification rate. First, more snowfall leads to more firn that can densify. Simulations with larger dt^{force} have more firn (Fig. 3), and therefore undergo more densification (Fig. 5 and Fig. 4, process 2).

Second, the densification is governed by the instantaneous layer temperature (T in Eq. 3) and the temperature of the bottom layer (T_b in Eq. 3), with higher T enhancing densification and higher T_b reducing it (Fig. 4, process 2). When both T and T_b increase, densification is enhanced (see constants Eq. 3). As the simulation with dt_{3h}^{force} has deeper refreezing (Fig. 7a compared to Fig. 7b) and warmer firn (Fig. 7c compared to Fig. 7d), the densification is indeed faster. An exception occurs

https://doi.org/10.5194/egusphere-2026-462
Preprint. Discussion started: 19 February 2026

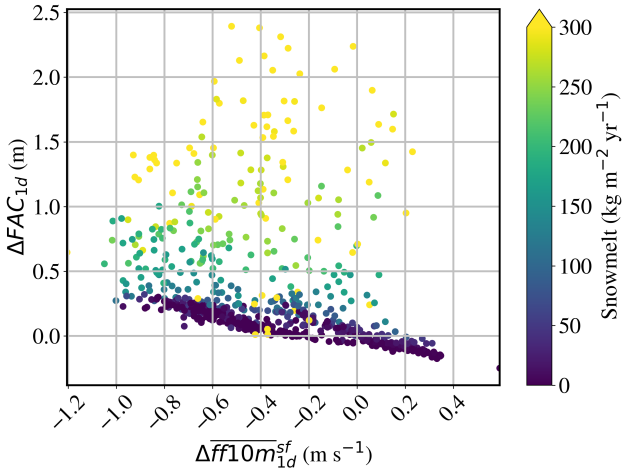

Figure 8. The ΔFAC_{1d} against $\Delta\overline{ff10m}^{sf}_{1d}$ in the APIS. $\Delta\overline{ff10m}^{sf}_{1d} = \overline{ff10m}^{sf}_{1d} - \overline{ff10m}^{sf}_{3h}$. In absence of melt, there is a clear relation between $\Delta\overline{ff10m}^{sf}_{1d}$ and ΔFAC_{1d}.

when T is similar for different dt^{force} for the uppermost meters of the firn column, but T_b is higher for dt^{force}_{3h} due to the deeper refreezing. Then the larger approximated grain size for dt^{force}_{3h} slows down the densification rate, leaving more FAC.

To summarize, higher firn temperatures at dt^{force}_{3h} increase densification rate, but overall densification remains lower as there is less firn.

3.2.3 Process 3: snowfall

An area with lower rather than higher ΔFAC is modelled in the APIS (red hues in Figs. 3b, c, and d); this relates to differences in the estimated fresh snow density for various dt^{force}. The simulation for dt^{force}_{3h} has more 10 m wind speed ff_{10m} variability than for larger dt^{force}, which influences fresh snow density through Eq. 1: fresh snow density increases with surface temperature T_s (Judson and Doesken, 2000) and ff_{10m} (Sato et al., 2008) (Fig. 4, process 3). The area with negative ΔFAC typically experiences snowfall at low ff_{10m}. Then, the snowfall-weighted average 10 m windspeed ($\overline{ff10m}^{sf}$) (Eq. 4) for dt^{force}_{3h} is lower than for higher dt^{force} (Fig. 8).

$$\overline{ff10m}^{sf} = \frac{\sum snowfall(t) * 10m - windspeed(t)}{\sum snowfall(t)} \tag{4}$$

Lower $\overline{ff10m}^{sf}_{3h}$ is related to lower fresh snow densities, and therefore higher FAC_{3h}. In climate zones with limited melt (< 30 kg m^{-2} yr^{-1}), this effect of the fresh snow density causes a relatively small ΔFAC of up to ± 0.5 m on typical FAC_{3h} values of 15-20 m (Figs. 3a, b, c, and d).

https://doi.org/10.5194/egusphere-2026-462
Preprint. Discussion started: 19 February 2026

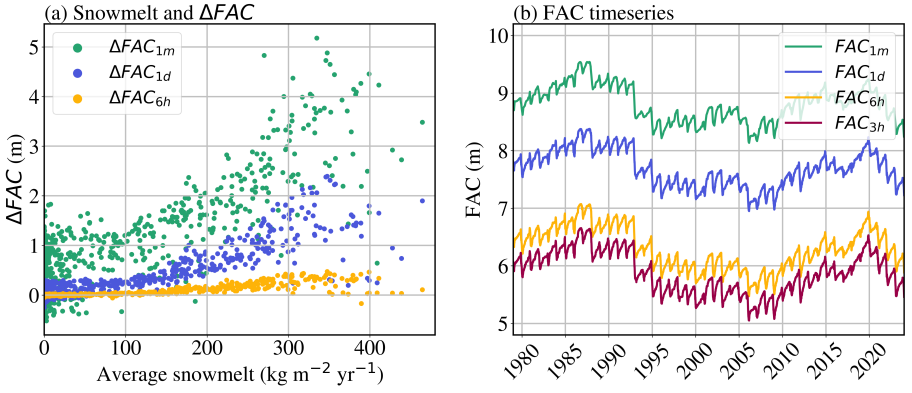

Figure 9. (a) Average ΔFAC_{6h}, ΔFAC_{1d}, and ΔFAC_{1m} over the simulation period against average snowmelt over 1979 - 2020. (b) FAC timeseries of one grid point on the APIS for the four dt^{force}. See Fig. 3a for a map with the grid cell location.

4 Implications ice sheets

Climatic differences between the APIS and southern GrIS lead to a different response of ΔFAC to dt^{force}. These implications are discussed in the following sections for both ice sheets.

4.1 APIS

Figure 9a shows that ΔFAC increases with snowmelt. Accordingly, ice shelves have largest positive ΔFAC values (Figs. 3b, c, and d), reflecting their relatively high snowmelt rates (Fig. 2b). Consequently, the chosen dt^{force} is crucial in assessing the vulnerability of an ice shelf in terms of firn air; neglecting the daily temperature and melt cycle in firn simulations could lead to underestimated ice shelf vulnerability.

Fig. 9b presents a FAC timeseries of a single grid cell on the Larsen C ice shelf (see Fig. 3 for location). The overall variations in FAC are similar across all simulations, with ΔFAC primarily established during the spin-up. This is in line with the expected behavior of firn layers. Although the main initial forcing to ΔFAC, namely reduced FAC removal during melt events for larger dt^{force}, is short-lived, the extra remaining FAC for dt^{force} is removed by enhanced densification on decadal timescales. Consequently, the equilibrium state of the firn column is with higher FAC for larger dt^{force}.

4.2 Southern GrIS

The wider range of climatic conditions in terms of snowmelt and accumulation in the southern GrIS (Fig. 10a) compared to the APIS (Fig. 9a), complicates the isolation of processes governing ΔFAC. To facilitate the discussion, we divide the accumulation-snowmelt space into four domains (Fig. 10a).

The largest increases in ΔFAC_{1d} occur at snowmelt rates of ~ 500 kg m^{-2} yr^{-1} and near a Melt-Over-Accumulation (MOA) ratio of 1 (Fig. 10a). Climate zones with snowmelt below 500 kg m^{-2} yr^{-1} (Fig. 10a, climate zone I), corresponding to

https://doi.org/10.5194/egusphere-2026-462
Preprint. Discussion started: 19 February 2026

the interior of the southern GrIS (Fig. 2e), behave similarly to the APIS: higher snowmelt rates increase ΔFAC_{1d}, with more ΔFAC gain for larger dt^{force}.

Firn aquifers can form when snowmelt exceeds 500 kg m^{-2} yr^{-1} (Kuipers Munneke et al., 2014; Brils et al., 2024). In climate zone II (Figs. 10a and b), which are the points with annual snowmelt between 500 and 800 kg m^{-2} yr^{-1}, firn aquifers formed under dt_{3h}^{force} during spin-up, but did not for dt_{1d}^{force}. As meltwater refreezing occurs deeper for dt_{3h}^{force}, the firn layer has a higher heat content. The higher heat content limits the refreezing capacity. We hypothesize that more liquid water remains in the firn layer and the aquifer can refill during the next melt season. In contrast, the cold content for dt_{1d}^{force} still facilitates refreezing of liquid water, and therefore, aquifers did not form during spin-up.

In climate zone III, snowmelt exceeds 800 kg m^{-2} yr^{-1} and the MOA is below 1. Firn aquifers form under both dt_{3h}^{force} and dt_{1d}^{force} (Fig. 10b). Here, ΔFAC_{1d} increases with snowmelt as more pore space is removed for larger dt^{force} (Fig. 4, process 1), but this process is increasingly counterbalanced by enhanced firn densification at sites with higher accumulation (Fig. 10a). FAC_{3h} is lower in this climate zone, so less pore space is available for water storage, resulting in less liquid water content (LWC) for dt_{3h}^{force} whereas the liquid water is still retained for dt_{1d}^{force} (Fig. 10b, climate zone III). More excess water for dt_{3h}^{force} leads to more runoff. This example illustrates that the runoff limit also depends on dt^{force} (Fig. 10c). In the southeastern GrIS, the runoff limit shifts more than 10 km inland for dt_{3h}^{force} compared to dt_{1d}^{force}, and up to 35 km compared to dt_{1m}^{force}.

When the MOA exceeds 1 (Fig. 10a climate zone IV), ΔFAC equals 0, as the firn is depleted in both simulations.

Unlike the example of the APIS (Fig. 9b), long-term FAC variability in Fig. 10d depends on dt^{force} (Fig. 10d). For dt_{3h}^{force}, firn aquifers are present at the start of the simulation, whereas for dt_{1d}^{force} they develop around 2005 (Fig. 10e). In this year, FAC_{1d} diverges from FAC_{3h}, and eventually, FAC_{1d} even drops below FAC_{3h}. This results from the densification equation (Eq. 3): liquid water in the aquifers sets the instantaneous temperature (T in Eq. 3) to 273.15 K. The bottom temperature (T_b in Eq. 3) is higher for dt_{3h}^{force} (section 3.2.1), because of the deeper refreezing and releasing of latent heat, slowing down densification. The faster densification under dt_{1d}^{force} reduces FAC_{1d}. Hence, for locations where aquifers form during the simulation, the time series of FAC (and surface elevation) become different and their trends possibly of opposite sign. This has important implications for the correct interpretation of satellite altimetry.

5 Lessons learned for firn modelling

In this section we present the lessons learned of using different dt^{force} in firn modelling. We distinguish between general findings and IMAU-FDM specifics.

First, we argue that firn models that prescribe snowmelt fluxes and surface temperature need at least a diurnal cycle in the dt^{force}. Snowmelt turned out to be the major predictor of ΔFAC, increasing ΔFAC for larger dt^{force}. Without resolving the daily cycle, snowmelt can co-exist with subfreezing surface temperatures, leading to immediate refreezing of meltwater. This decoupling of surface temperature and snowmelt leads to non-physical results.

https://doi.org/10.5194/egusphere-2026-462
Preprint. Discussion started: 19 February 2026

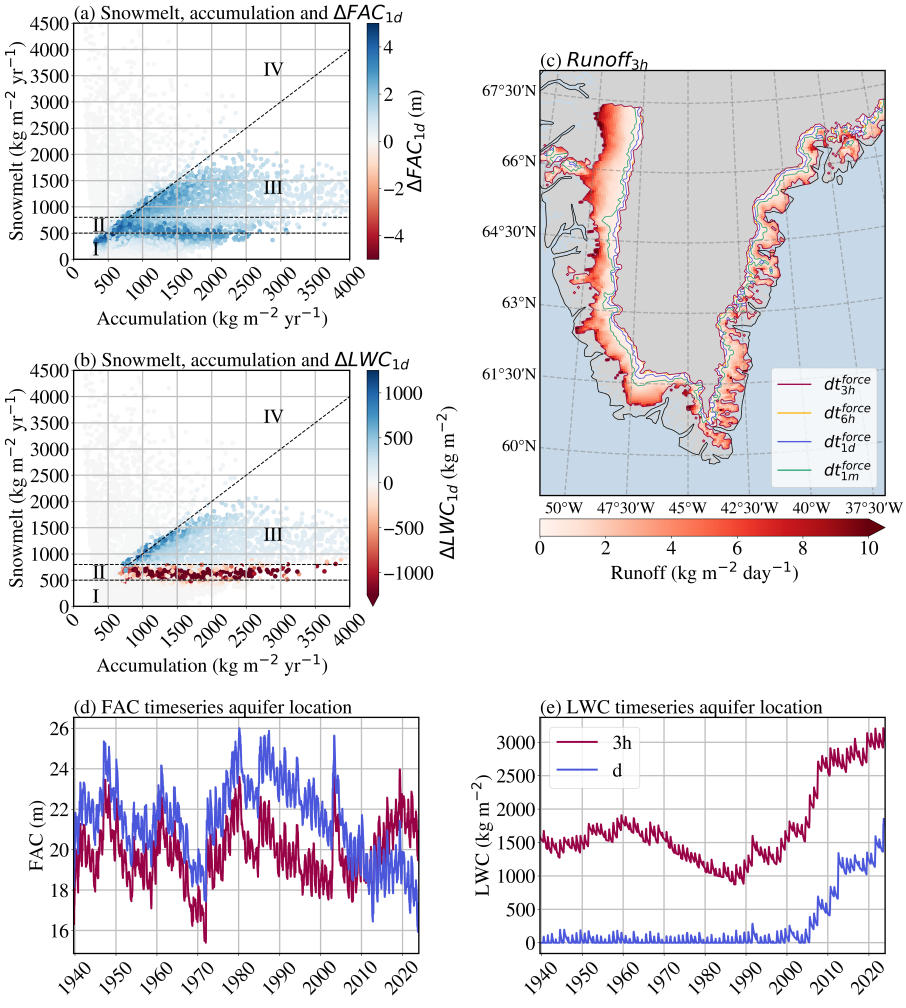

Figure 10. Average snowmelt against accumulation over 1939-1970 colour coded with average ΔFAC_{1d} (a) and ΔLWC_{1d} (b) over the simulation period. The black dashed lines represent snowmelt of 500 kg m^{-2} yr^{-1} (climate zone I), 500-800 kg m^{-2} yr^{-1} (climate zone II) and a MOA of 1 (separating climate zones III and IV). Panel (c) shows the average runoff$_{3h}$ over the simulation period and the different runoff limits for the four dt^{force}. Panel (d) and (e) show timeseries of respectively FAC_{3h} and FAC_{1d}, and LWC_{3h} and LWC_{1d}. See Fig. 3e for a map with the grid cell location.

Second, a general lesson learned for modelling is that the original purpose and forcing time step of a parameterization should be respected when applying it. The fresh-snow density parameterization (Eq. 1) in the APIS is an example where the parameterization is tuned specifically using dt_{3h}^{force} (Veldhuijsen et al., 2023). ΔFAC arising from other dt^{force} are related to the parameterization (Fig. 8) and are not based on physical grounds. We also gave an example of the densification equation (Eq. 3) which is based on steady state and dry assumptions. However, we applied the parameterization at larger dt^{force} and transient and wet conditions. The latter results in non-physical processes where the bottom temperature (T_b in Eq. 3) determines

https://doi.org/10.5194/egusphere-2026-462
Preprint. Discussion started: 19 February 2026

the densification rate in an aquifer and leads to different FAC trends when the model is forced at dt_{3h}^{force} or dt_{1d}^{force} (Figs. 10d and e).

6 Conclusions

Ice-sheet firn models in literature use different surface climate forcing time steps. We investigated the effect on firn air content of a 3-hour, 6-hour, 1-day, and 1-month climate forcing time step on IMAU-FDM in the APIS and southern GrIS. We find that increasing the climate forcing time step usually results in more firn air (ΔFAC). The strongest sensitivities are found in climate zones with low FAC_{3h} or where firn aquifers are absent under larger forcing time steps, but present under shorter ones. ΔFAC resulting from the forcing time step is governed by snowmelt, firn densification, and snowfall. More specifically, (1) snowmelt is the main contributor to the positive ΔFAC. Input data requires a diurnal cycle when surface temperature and snowmelt are prescribed to a firn model. Otherwise, subfreezing temperatures and snowmelt can coexist, leading to immediate refreezing of the water and, consequently, overestimating the amount of firn air; (2) parameterizations should be applied respecting their original purpose and temporal resolution. The fresh snow density parameterization determined the ΔFAC under limited snowmelt conditions and is related to dt^{force} on non-physical grounds. The densification parameterization leads to non-physical FAC for all dt^{force} when applied in wet conditions. (3) the climate forcing time step is critical in assessing ice shelf vulnerability in APIS, the runoff limit in the GrIS, and the interpretation of altimetry observations.

Code and data availability. IMAU-FDM code will be released on GIT with final submission. The code to create the figures will also be made available on GIT. The datasets will be published on Zenodo.

Author contributions. TvdA, PKM, WJvdB and MvdB designed the study. TvdA performed and analyzed the simulations. All co-authors contributed to discussions on the research and manuscript.

Competing interests. At least one of the (co-)authors is a member of the editorial board of *The Cryosphere*. The authors have no other competing interests to declare.

Acknowledgements. This work was supported by EMBRACER (Summit grant no. SUMMIT.1.034), financed by the Netherlands Organization for Scientific Research (NWO). We acknowledge ECMWF for computational time on their supercomputers. We would like to thank Sanne Veldhuijsen for the origin of the idea for this project during the MSc thesis supervision, and Elizabeth Case for the improvements and development on IMAU-FDM. ChatGPT is used for figure formatting.

https://doi.org/10.5194/egusphere-2026-462
Preprint. Discussion started: 19 February 2026

References

Arthern, R. J., Vaughan, D. G., Rankin, A. M., Mulvaney, R., and Thomas, E. R.: In situ measurements of Antarctic snow compaction compared with predictions of models, Journal of Geophysical Research: Earth Surface, 115, https://doi.org/10.1029/2009JF001306, 2010.

Brils, M., Kuipers Munneke, P., van de Berg, W. J., and van den Broeke, M.: Improved representation of the contemporary Greenland ice sheet firn layer by IMAU-FDM v1. 2G, Geoscientific Model Development, 2021, 1–28, https://doi.org/10.5194/gmd-15-7121-2022, 2021.

Brils, M., Munneke, P. K., Jullien, N., Tedstone, A., Machguth, H., Van De Berg, W., and Van Den Broeke, M.: Climatic drivers of ice slabs and firn aquifers in Greenland, Geophysical Research Letters, 51, e2023GL106 613, https://doi.org/10.1029/2023GL106613, 2024.

Calonne, N., Milliancourt, L., Burr, A., Philip, A., Martin, C. L., Flin, F., and Geindreau, C.: Thermal conductivity of snow, firn, and porous ice from 3-D image-based computations, Geophysical Research Letters, 46, 13 079–13 089, https://doi.org/10.1029/2019GL085228, 2019.

Coléou, C. and Lesaffre, B.: Irreducible water saturation in snow: experimental results in a cold laboratory, Annals of glaciology, 26, 64–68, https://doi.org/10.3189/1998AoG26-1-64-68, 1998.

Fausto, R. S., Box, J. E., Vandecrux, B., Van As, D., Steffen, K., MacFerrin, M. J., Machguth, H., Colgan, W., Koenig, L. S., McGrath, D., et al.: A snow density dataset for improving surface boundary conditions in Greenland ice sheet firn modeling, Frontiers in Earth Science, 6, 51, https://doi.org/10.3389/feart.2018.00051, 2018.

Gkinis, V., Holme, C., Kahle, E. C., Stevens, M. C., Steig, E. J., and Vinther, B. M.: Numerical experiments on firn isotope diffusion with the Community Firn Model, Journal of Glaciology, 67, 450–472, https://doi.org/10.1017/jog.2021.1, 2021.

Hansen, N., Orr, A., Zou, X., Boberg, F., Bracegirdle, T. J., Gilbert, E., Langen, P. L., Lazzara, M. A., Mottram, R., Phillips, T., et al.: The importance of cloud properties when assessing surface melting in an offline-coupled firn model over Ross Ice shelf, West Antarctica, The Cryosphere, 18, 2897–2916, https://doi.org/10.5194/tc-18-2897-2024, 2024.

Helsen, M. M., Van Den Broeke, M. R., Van De Wal, R. S., Van De Berg, W. J., Van Meijgaard, E., Davis, C. H., Li, Y., and Goodwin, I.: Elevation changes in Antarctica mainly determined by accumulation variability, science, 320, 1626–1629, https://doi.org/10.1126/science.1153894, 2008.

Hersbach, H., Bell, B., Berrisford, P., Hirahara, S., Horányi, A., Muñoz-Sabater, J., Nicolas, J., Peubey, C., Radu, R., Schepers, D., et al.: The ERA5 global reanalysis, Quarterly journal of the royal meteorological society, 146, 1999–2049, https://doi.org/10.1002/qj.3803, 2020.

Judson, A. and Doesken, N.: Density of freshly fallen snow in the central Rocky Mountains, Bulletin of the American Meteorological Society, 81, 1577–1588, https://doi.org/10.1175/1520-0477(2000)081<1577:DOFFSI>2.3.CO;2, 2000.

Kuipers Munneke, P., M. Ligtenberg, S., Van Den Broeke, M., Van Angelen, J., and Forster, R.: Explaining the presence of perennial liquid water bodies in the firn of the Greenland Ice Sheet, Geophysical Research Letters, 41, 476–483, https://doi.org/10.1002/2013GL058389, 2014.

Kuipers Munneke, P., Ligtenberg, S., Noël, B., Howat, I., Box, J., Mosley-Thompson, E., McConnell, J., Steffen, K., Harper, J., Das, S., et al.: Elevation change of the Greenland Ice Sheet due to surface mass balance and firn processes, 1960–2014, The Cryosphere, 9, 2009–2025, https://doi.org/10.5194/tc-9-2009-2015, 2015.

Langen, P. L., Fausto, R. S., Vandecrux, B., Mottram, R. H., and Box, J. E.: Liquid water flow and retention on the Greenland ice sheet in the regional climate model HIRHAM5: Local and large-scale impacts, Frontiers in Earth Science, 4, 110, https://doi.org/10.3389/feart.2016.00110, 2017.

https://doi.org/10.5194/egusphere-2026-462
Preprint. Discussion started: 19 February 2026

Lenaerts, J. T., Van den Broeke, M., Déry, S., Van Meijgaard, E., Van de Berg, W., Palm, S. P., and Sanz Rodrigo, J.: Modeling drifting snow in Antarctica with a regional climate model: 1. Methods and model evaluation, Journal of Geophysical Research: Atmospheres, 117, https://doi.org/10.1029/2011JD016145, 2012.

Ligtenberg, S., Helsen, M., and Van den Broeke, M.: An improved semi-empirical model for the densification of Antarctic firn, The Cryosphere, 5, 809–819, https://doi.org/10.5194/tc-5-809-2011, 2011.

Ligtenberg, S., Kuipers Munneke, P., and Van den Broeke, M.: Present and future variations in Antarctic firn air content, The Cryosphere, 8, 1711–1723, https://doi.org/10.5194/tc-8-1711-2014, 2014.

Medley, B., Neumann, T. A., Zwally, H. J., Smith, B. E., and Stevens, C. M.: Simulations of firn processes over the Greenland and Antarctic ice sheets: 1980–2021, The Cryosphere, 16, 3971–4011, https://doi.org/10.5194/tc-16-3971-2022, 2022.

Meyer, C. R. and Hewitt, I. J.: A continuum model for meltwater flow through compacting snow, The Cryosphere, 11, 2799–2813, https://doi.org/10.5194/tc-11-2799-2017, 2017.

Noël, B., Van De Berg, W. J., Van Wessem, J. M., Van Meijgaard, E., Van As, D., Lenaerts, J., Lhermitte, S., Kuipers Munneke, P., Smeets, C., Van Ulft, L. H., et al.: Modelling the climate and surface mass balance of polar ice sheets using RACMO2–Part 1: Greenland (1958–2016), The Cryosphere, 12, 811–831, https://doi.org/10.5194/tc-12-811-2018, 2018.

Noël, B., Lenaerts, J. T., Lipscomb, W. H., Thayer-Calder, K., and van den Broeke, M. R.: Peak refreezing in the Greenland firn layer under future warming scenarios, Nature Communications, 13, 6870, https://doi.org/10.1038/s41467-022-34524-x, 2022.

Sato, T., Kosugi, K., Mochizuki, S., and Nemoto, M.: Wind speed dependences of fracture and accumulation of snowflakes on snow surface, Cold Regions Science and Technology, 51, 229–239, https://doi.org/10.1016/j.coldregions.2007.05.004, international Snow Science Workshop (ISSW) 2006, 2008.

Shepherd, A., Ivins, E. R., A, G., Barletta, V. R., Bentley, M. J., Bettadpur, S., Briggs, K. H., Bromwich, D. H., Forsberg, R., Galin, N., et al.: A reconciled estimate of ice-sheet mass balance, Science, 338, 1183–1189, https://doi.org/10.1126/science.1228102, 2012.

Simonsen, S. B., Stenseng, L., Adalgeirsdottir, G., Fausto, R. S., Hvidberg, C. S., and Lucas-Picher, P.: Assessing a multilayered dynamic firn-compaction model for Greenland with ASIRAS radar measurements, Journal of Glaciology, 59, 545–558, https://doi.org/10.3189/2013JoG12J158, 2013.

Sørensen, L. S., Simonsen, S. B., Nielsen, K., Lucas-Picher, P., Spada, G., Adalgeirsdottir, G., Forsberg, R., and Hvidberg, C. S.: Mass balance of the Greenland ice sheet (2003–2008) from ICESat data–the impact of interpolation, sampling and firn density, The Cryosphere, 5, 173–186, https://doi.org/10.5194/tc-5-173-2011, 2011.

Stevens, C. M., Verjans, V., Lundin, J. M., Kahle, E. C., Horlings, A. N., Horlings, B. I., and Waddington, E. D.: The community firn model (cfm) v1. 0, Geoscientific Model Development, 2020, 1–37, https://doi.org/10.5194/gmd-13-4355-2020, 2020.

The Firn Symposium team: Firn on ice sheets, Nature Reviews Earth & Environment, 5, 79–99, https://doi.org/10.1038/s43017-023-00507-9, 2024.

Thompson-Munson, M., Wever, N., Stevens, C. M., Lenaerts, J., and Medley, B.: An evaluation of a physics-based firn model and a semi-empirical firn model across the Greenland Ice Sheet (1980–2020), The Cryosphere, 17, 2185–2209, https://doi.org/10.5194/tc-17-2185-2023, 2023.

Van Wessem, J. M., Van De Berg, W. J., Noël, B. P., Van Meijgaard, E., Amory, C., Birnbaum, G., Jakobs, C. L., Krüger, K., Lenaerts, J., Lhermitte, S., et al.: Modelling the climate and surface mass balance of polar ice sheets using RACMO2–Part 2: Antarctica (1979–2016), The Cryosphere, 12, 1479–1498, https://doi.org/10.5194/tc-12-1479-2018, 2018.

https://doi.org/10.5194/egusphere-2026-462
Preprint. Discussion started: 19 February 2026

Vandecrux, B., Mottram, R., Langen, P. L., Fausto, R. S., Olesen, M., Stevens, C. M., Verjans, V., Leeson, A., Ligtenberg, S., Kuipers Munneke, P., et al.: The firn meltwater Retention Model Intercomparison Project (RetMIP): evaluation of nine firn models at four weather station sites on the Greenland ice sheet, The Cryosphere, 14, 3785–3810, https://doi.org/10.5194/tc-14-3785-2020, 2020.

Veldhuijsen, S., van de Berg, W. J., Brils, M., Kuipers Munneke, P., and van den Broeke, M. R.: Characteristics of the 1979–2020 Antarctic firn layer simulated with IMAU-FDM v1. 2A, The Cryosphere, 17, 1675–1696, https://doi.org/10.5194/tc-17-1675-2023, 2023.

Verjans, V., Leeson, A. A., Stevens, C. M., MacFerrin, M., Noël, B., and Van Den Broeke, M. R.: Development of physically based liquid water schemes for Greenland firn-densification models, The Cryosphere, 13, 1819–1842, https://doi.org/10.5194/tc-13-1819-2019, 2019.

Wang, W., Shen, Y., Chen, Q., and Wang, F.: Unprecedented mass gain over the Antarctic ice sheet between 2021 and 2022 caused by large precipitation anomalies, Environmental Research Letters, 18, 124 012, https://doi.org/10.1088/1748-9326/ad0863, 2023.

Wever, N., Keenan, E., Amory, C., Lehning, M., Sigmund, A., Huwald, H., and Lenaerts, J. T.: Observations and simulations of new snow density in the drifting snow-dominated environment of Antarctica, Journal of Glaciology, 69, 823–840, https://doi.org/10.1017/jog.2022.102, 2023.

Winther, J.-G., Jespersen, M. N., and Liston, G. E.: Blue-ice areas in Antarctica derived from NOAA AVHRR satellite data, Journal of Glaciology, 47, 325–334, https://doi.org/10.3189/172756501781832386, 2001.

Zhang, X., Liu, L., Noël, B., and Luo, Z.: Modelling firn density at Dye-2 and KAN_U, two sites in the percolation zone of the Greenland ice sheet, EGUsphere [preprint], 2024, 1–37, https://doi.org/10.5194/egusphere-2024-1726, 2024.